Progress In Electromagnetics Research C, Vol. 57, 1–12, 2015

Dual-Band Substrate Integrated Waveguide Resonator Based on Sierpinski Carpet

Michele A. Chiapperino[1], Onofrio Losito[1], Tiziana Castellano[1], Giuseppe Venanzoni[1], Luciano Mescia[1], Giacomo Angeloni[2], Chiara Renghini[2], Pasquale Carta[2], Paolo Potenza[2], and Francesco Prudenzano[1, *]

Abstract—In this paper, a dual-band Substrate Integrated Waveguide (SIW) resonator with Sierpinski fractal geometry is proposed. The space-filling property of the employed fractal shape allows to reduce the resonator size. The bandwidth, the minimum insertion loss, the maximum return loss and the stop band rejection are considered for evaluating the effect of the fractal geometry on the resonator characteristics. An accurate electromagnetic investigation is made using a full wave finite element method solver (Ansoft HFSS). Simulated and measured results are in good agreement. The second iteration fractal resonator exhibits two simulated bands centered at the frequencies $f_1 = 11.57\,\text{GHz}$ and $f_2 = 25.7\,\text{GHz}$, while the measured frequencies are $f_1 = 11.33\,\text{GHz}$, $f_2 = 23.67\,\text{GHz}$. The measured bandwidths are $\text{BW} = 1.15\,\text{GHz}$ and $\text{BW} = 2\,\text{GHz}$ and the minimum insertion losses are close to $-1.36\,\text{dB}$ and $-1.97\,\text{dB}$, respectively. The prototypes of the square resonator without, with first and with second iteration fractal geometry are fabricated via standard printed circuit board process (PCB). A Rogers Duroid 5880 substrate with thickness $t = 0.381\,\text{mm}$ is employed.

1. INTRODUCTION

Modern wireless local-area networks (WLAN), local multipoint distributions systems (LMDS), satellite communications, radar applications, remote sensing and global positioning systems are stimulating an increasing need for high performance, compact and low-loss microwave devices [1]. Since conventional waveguide components cannot be directly integrated with microwave or millimeter wave planar integrated circuits, substrate integrated waveguides (SIWs) are considered a valid alternative for the fabrication of high compactness, microwave and millimeter wave, integrated circuits. In fact, SIW devices, obtained by employing metallic-via arrays in conventional dielectric substrate, can be easily integrated within microwave and millimeter wave circuits by employing standard printed circuit board (PCB) process. Moreover, because the electromagnetic field distribution in a SIW is similar to that occurring in a conventional rectangular waveguide, high Q-factor, low insertion loss and high-power components can be designed. Therefore, the SIW technology has been largely investigated and used for the construction of several microwave devices, including active circuits, passive components, and antennas [1–5].

During the last decades a variety of SIW cavity filters have been proposed in literature, following different design approaches [6–13]. Different resonator shapes have been employed, such as rectangular [5, 6], circular [7] and triangular ones [9, 10]. In particular, the coupling matrix method has been used in order to design different filters based on triangular cavities, cascading blocks and multilayer structures. Contour integral and symmetrical window methods have been considered in filter

Received 13 November 2014, Accepted 22 December 2014, Scheduled 9 April 2015
* Corresponding author: Francesco Prudenzano (francesco.prudenzano@poliba.it).
[1] DEI-Dipartimento di Ingegneria Elettrica e dellInformazione, Politecnico di Bari, Via E. Orabona 4, Bari 70125, Italy. [2] R&D Department, Somacis Spa, Via Jesina 17, Castelfidardo 60022, Italy.

design [6]. Cross-coupled resonators have been employed to increase selectivity [11–13]. In [13] the design of a microwave band pass filter with frequency-dependent coupling, via substrate integrated waveguide (SIW) technology, has been proposed. The increasing demand for wireless communication applications requires radio frequency transceivers with dual-band or multi-band operation, allowing the access to more services with a single handset [10, 14]. In [14] a stub-loaded quad-mode resonator has been proposed. The quad-mode resonator had a compact size and two pass bands operating at 1.5 and 2.4 GHz.

In order to minimize the size of a planar filter, fractal technique is often used [15–19]. Fractal geometries refer to highly complex structures, e.g., those of clouds, ocean floor, biological tissues, which cannot be described by the conventional Euclidean geometry. However, a fractal geometry can be identified with few parameters because all fractals are self-similar and repeat themselves at different scales. Filters can be reduced in sizes by applying fractal rules to their layout [16, 17]. In fact, fractals allow to create longer current lines on smaller surfaces. In [15] a low-pass filter with stubs separated by transmission lines over the ground plane with a fractal defected ground (DGS) structure has been proposed. For a six-element fractal DGS, the dimension has been reduced by 22.43% compared to the filter over the solid ground plane.

In this paper, a novel dual-band SIW filter employing a Sierpinski fractal geometry is proposed. The filter is based on a square quarter mode resonator. The novelty of the paper lies in the combined use of fractal geometry, SIW technology, quarter mode approach. This strategy has allowed to reduce the size of the resonator (via fractal geometry and quarter mode approach) and to obtain a suitable bounding of the electromagnetic field, similar to that occurring in rectangular waveguides (via SIW technology). The design is performed by using the full wave simulator Ansoft HFSS. The effect of the fractal iterations on the resonator characteristics are investigated. SIW filters are fabricated via a single-layer PCB process in SOMACIS. The paper is organized as follows: Section 1, the introduction; Section 2, a brief introduction on fractals; Section 3, the design; Section 4, the experimental results; Section 5, the conclusion.

2. SIERPINSKI FRACTAL GEOMETRY

Fractal geometries are characterized by the self-similarity property repeating themselves at different scales [18–20]. Basic fractal techniques are Koch, Minkowski, Sierpinski and Hilbert ones. The construction of the Sierpinski geometry (carpet) is obtained by dividing a square, see Figure 1(a), in nine congruent sub-squares (dashed white lines) and by eliminating the central sub-square as in Figure 1(b). Therefore, eight sub-squares arrange the 1st iteration fractal geometry of Figure 1(b). By repeating this procedure on the remaining eight sub-squares, the 2nd iteration fractal geometry of Figure 1(c) and the 3rd iteration fractal one of Figure 1(d) are obtained.

Figure 1. Sierpinski carpet fractal geometry: (a) Square without fractal; (b) 1st iteration fractal; (c) 2nd iteration fractal; (d) 3rd iteration fractal geometry.

The fractal dimension D_{Nr} is a number related to the irregularity grade of the fractal geometry:

$$D_{Nr} = \frac{\log N}{\log\left(\frac{1}{r}\right)} \tag{1}$$

where N is the number of remaining subparts forming the geometry after a single fractal rule application and r the self-similarity ratio. For Sierpinski fractal rule, $N = 8$ and $r = 1/3$; by applying Equation (1) the fractal dimension is $D = 1.89$. For a square with side 1, after the n-th Sierpinski rule iteration, the area and perimeter of the obtained fractal geometry are:

$$A_n = \left(\frac{8}{9}\right)^n A_0 \tag{2}$$

$$p_n = p_0 \left(1 + \sum_{i=1}^{n} \frac{8^{i-1}}{3^i}\right) \tag{3}$$

where A_0 and p_0 are the area and the perimeter of the starting square, respectively. As expected, by the inspection of Figure 1, for $n \to \infty$, A_n and p_n tend to 0 and ∞, respectively [18].

3. RESONATOR DESIGN

Half-mode substrate integrated waveguides (HMSIWs) have been proposed in literature in order to reduce the size of SIW devices. This technique enables the size reduction of the substrate integrated waveguide devices nearly in half without deteriorating their performance [21–24]. The concept of quarter mode SIW (QMSIW) can be applied for obtaining a further size reduction [23, 24]. As an example, Figure 2 illustrates the modulus of the electromagnetic field distribution of the dominant mode in (a) conventional square SIW Resonator (SIWR) and (b) Quarter SIW Resonator (QSIWR). In the HFSS simulation a single layer Rogers Duroid 5880 with dielectric constant $\varepsilon_r = 2.2$, loss tangent $\delta = 0.0009$ and thickness $t = 0.381$ mm has been considered. The SIWR walls, see Figure 2(a), are: i) the substrate metallic ground plane; ii) the top metalized, square shaped, area; and iii) the four sides obtained by means of the metalized via holes. The QSIWR walls, see Figure 2(b), are: i) the substrate metallic ground plane; ii) the top metalized, square shaped, area (which is a quarter of the top metalized one of SIWR); iii) the two sides obtained by means of the metalized via holes and iv) the other two sides 1, 2 which are open (i.e., without metalized via walls). The values of the side length of the square resonator, the diameter of metalized via holes and the center to center pitch between two adjacent metalized vias, will be discussed in the following. The Figure 2 is here qualitatively reported in order to evidence that the QSIWR electromagnetic field distribution can be obtained by cutting the SIW square resonator along two fictitious magnetic walls (dark dashed lines), i.e., along its symmetrical planes. This approach has been followed in [24], for a conventional (with all the walls made of metalized planes and not obtained through metalized vias) rectangular cavity.

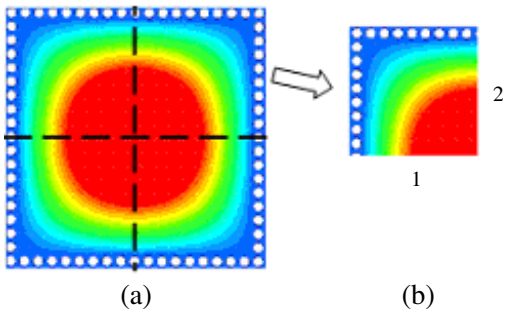

Figure 2. Top view of the (a) conventional square SIWR cavity and (b) the proposed QSIWR.

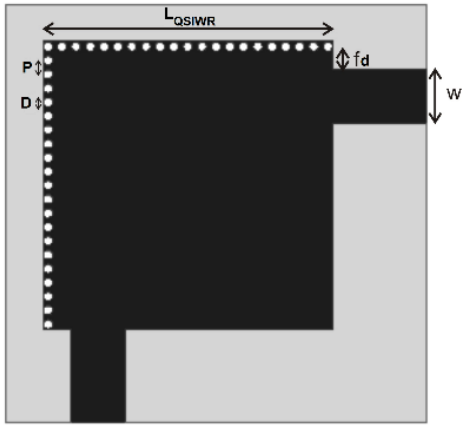

Figure 3. Layout of the SIW resonator without fractal geometry.

The resonant frequency $f_{n,m,l}$ of the n, m, l resonant mode in a conventional rectangular cavity is:

$$f_{n,m,l} = \frac{c_0}{\sqrt{\varepsilon_r}} \left[\left(\frac{1}{2d}\right)^2 + \left(\frac{m}{2b}\right)^2 + \left(\frac{n}{2a}\right)^2 \right]^{\frac{1}{2}} \tag{4}$$

where c_0 is the velocity of light in free space, ε_r the relative permittivity of the substrate, a the width, b the height, and d the length of the resonant cavity.

The geometry of QSIWR is a square, (see Figure 2(b)), having half size compared to that of the square SIWR cavity of Figure 2(a)), with resonant frequency:

$$f_{n,m,l} = \frac{c_0}{\sqrt{\varepsilon_r}} \left[\left(\frac{l}{2L_{\mathit{eff}}}\right)^2 + \left(\frac{m}{2t}\right)^2 + \left(\frac{n}{2L_{\mathit{eff}}}\right)^2 \right]^{\frac{1}{2}} \tag{5}$$

where t is the dielectric layer thickness and L_{eff} the equivalent length of SIW cavity, obtained by the following expression:

$$L_{\mathit{eff}} = 2L_{\mathrm{QSIWR}} - \frac{D^2}{0.95P} \tag{6}$$

where L_{QSIWR}, D and P are the side length of the quarter SIW resonator, the diameter of metalized via holes and the center to center pitch between two adjacent metalized vias, respectively [8].

Leakage losses are minimized when Equation (7) are simultaneously satisfied [25]:

$$\frac{P}{D} < 2 \quad \text{and} \quad \frac{D}{2L_{\mathrm{QSIWR}}} < \frac{1}{5} \tag{7}$$

The resonant frequency of the dominant mode TE_{101} of QSIWR is:

$$f_r = \frac{c_0}{L_{\mathit{eff}}\sqrt{2\varepsilon_r}} \tag{8}$$

The Rogers Duroid 5880 single layer, with dielectric constant $\varepsilon_r = 2.2$, loss tangent $\delta = 0.0009$ and thickness $t = 0.381$, is employed for the design and fabrication of the resonator. The configuration of the

Table 1. Resonator optimized parameter.

Parameter	**Dimension (mm)**
D	0.2
P	0.3
w	1.155
f_d	0.4
L_{QSIWR}	6

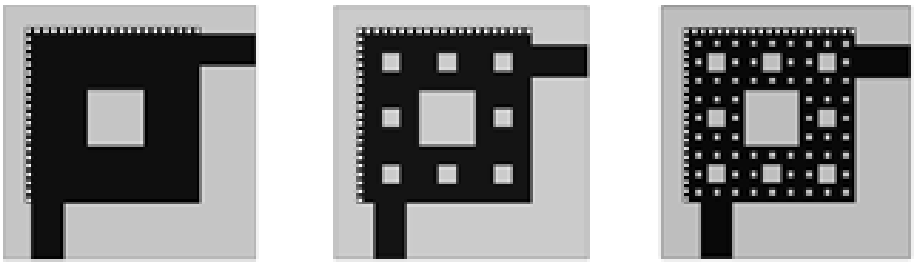

(a) (b) (c)

Figure 4. Different iteration fractal SIW resonators, (a) 1st iteration, (b) 2nd iteration, (c) 3rd iteration.

SIW resonator without fractal geometry is shown in Figure 3. The resonator input/output feeding lines are two microstrips with characteristic impedance $Z_0 = 50\,\Omega$, set at the square open sides, i.e., the two sides without the SIW wall. As the first design step, the size of the square resonator without fractal has been determined by applying Equations (5)–(8) to obtain the resonant frequency of the dominant mode close to $f_r = 11.8\,\text{GHz}$. Then, a fine optimization is made by using the Ansoft HFSS software. Table 1 reports the optimized geometry parameters. The electromagnetic investigation is performed for different iteration (1th–3rd) fractal SIW resonators, whose structures are reported in Figure 4. The resonators have a double-band response. For shortness, details on the investigation approach are reported only for the second iteration fractal resonator. The effect of the feed distance f_d on the two bandwidths, pertaining to the first and second frequency band, has been investigated. More precisely, Figure 5(a) illustrates the second iteration fractal SIW resonator bandwidths as a function of the feed distance in the range from $f_d = 0\,\text{mm}$ to $f_d = 1.4\,\text{mm}$. The bandwidth increases for both first and second bands by increasing f_d.

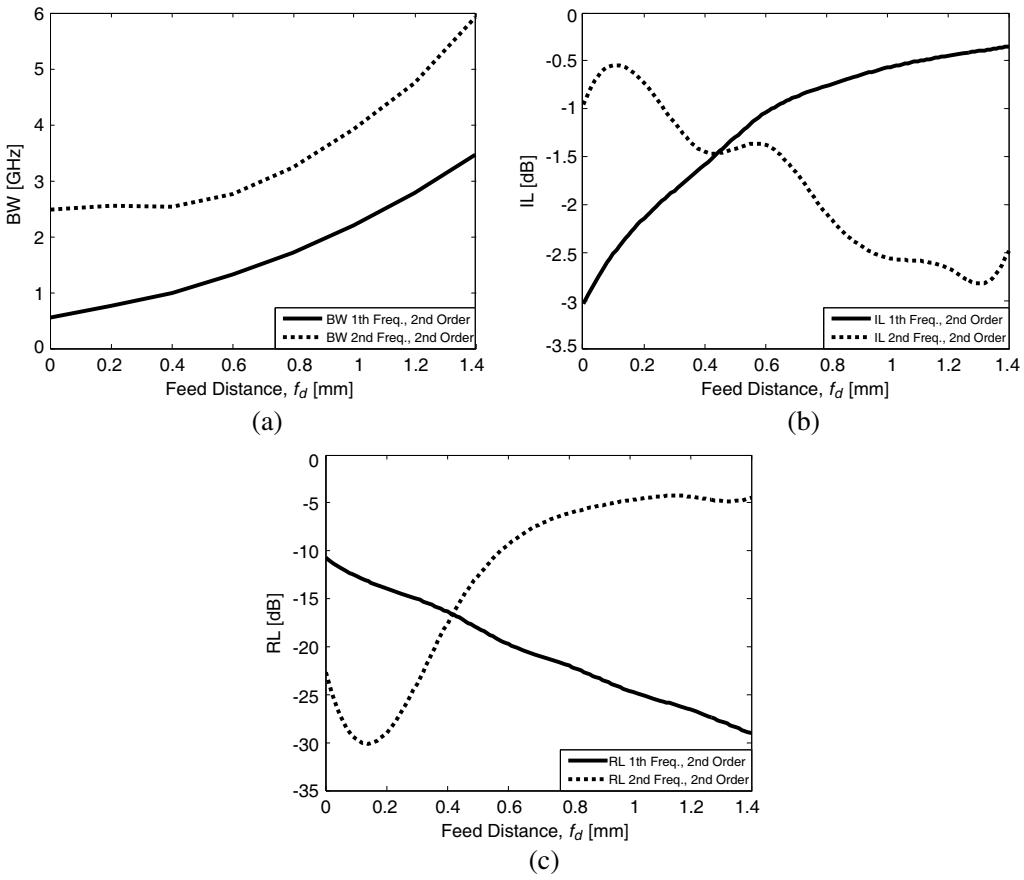

Figure 5. (a) Bandwidth, (b) insertion loss and (c) return loss versus feed distance f_d for the 2nd iteration fractal resonator.

Figure 5(b) illustrates the insertion loss IL versus f_d. By increasing f_d, the IL increases for the first band and decreases for the second band. Figure 5(c) illustrates the return loss RL versus the distance f_d. RL decreases for the first band and increases for the second band. To reach a good compromise for all the parameters pertaining to both bands, for the second iteration fractal resonator, a feed distance $f_d = 0.4\,\text{mm}$ is chosen. This value allows good performance also for the other fractal orders. Therefore, the same feed distance is also used for all the other resonators.

The external quality factor is calculated by using the following equation [19]:

$$Q_e = \frac{\tau_{s_{11}} 2\pi f_0}{2} \tag{9}$$

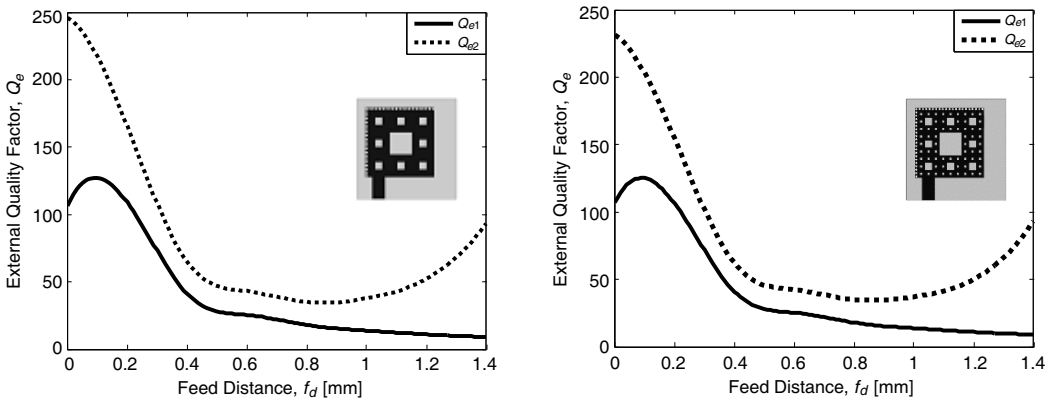

Figure 6. External quality factor Q_e versus feed distance f_d, for (a) the second iteration fractal resonator and (b) the third iteration fractal resonator.

where $\tau_{S_{11}}$ is the group delay of scattering parameter S_{11} at the resonant frequency f_0. Figure 6(a) and Figure 6(b) report the calculated external quality factor Q_e versus the feeding distance f_d for the second and third iteration fractal resonators, where Q_{e1} and Q_{e2} are the external quality factors corresponding to the first and second resonant frequencies, respectively.

Both the second and third iteration fractal resonators are characterized by high quality factors in each of two bands, and they decrease by increasing the feed distance till $f_d = 1\,\text{mm}$. For feed distance longer than $f_d = 1\,\text{mm}$ the Q_{e2} quality factor increases.

In Table 2 the external quality factors in the first and second bands are reported for different iterations fractal resonators for the feed distance $f_d = 0.4\,\text{mm}$. By increasing the resonator fractal iteration, the first band external quality factor Q_{e1} decreases, even if it remains high.

Table 2. External quality factors for the different iterations fractal resonators $F_D = 0.4\,\text{mm}$.

Resonator parameters	***Zero Order***	***First Order***	***Second Order***	***Third Order***
Q_{e1}	66.75	44.98	41.33	40.87
Q_{e2}	17.84	77.99	64.91	62.2

The second band external quality factor Q_{e2} significantly increases, which indicates an improvement of the filtering in the second band. The second and third iteration fractal resonators have quite similar values. Figures 7(a)–7(d) show the simulated IL and RL in the frequency range from 5 GHz to 30 GHz, for different iteration fractal resonators. For the resonator without fractal, see Figure 7(a), the first band is centered at 11.84 GHz, while the second band is not well defined. By introducing the fractal technique, the dual-band operation is obtained as apparent in Figure 7(b). For the second fractal iteration, see Figure 7(c), an improvement of the first band resonator performance occurs, and the second bandwidth is slightly narrower. The third iteration fractal resonator response is illustrated in Figure 7(d). There is a further improvement of the first band resonator parameters, and the features of the second band remain almost unchanged compared to the second iteration fractal resonator.

The different behaviors of frequency response of the resonator depend on the fractal order. In fact, fractal geometry provides an increasing number of the density current paths; this can allow the circuit miniaturization and can improve the filtering performance [19]. Figures 8(a)–8(c) illustrate the effect of the fractal geometry on the current density lines, simulated at the first band central frequency, for different fractal orders. The central first band frequencies are $f_1 = 11.84\,\text{GHz}$, $f_1 = 11.59\,\text{GHz}$, $f_1 = 11.57\,\text{GHz}$, for the zero, first and second fractal iteration, respectively. Similar results are found for the third iteration fractal resonator.

Tables 3–4 report the simulated parameters, for the different fractal geometries pertaining to the first and second band, respectively. They report the resonant frequency, bandwidth, maximum insertion

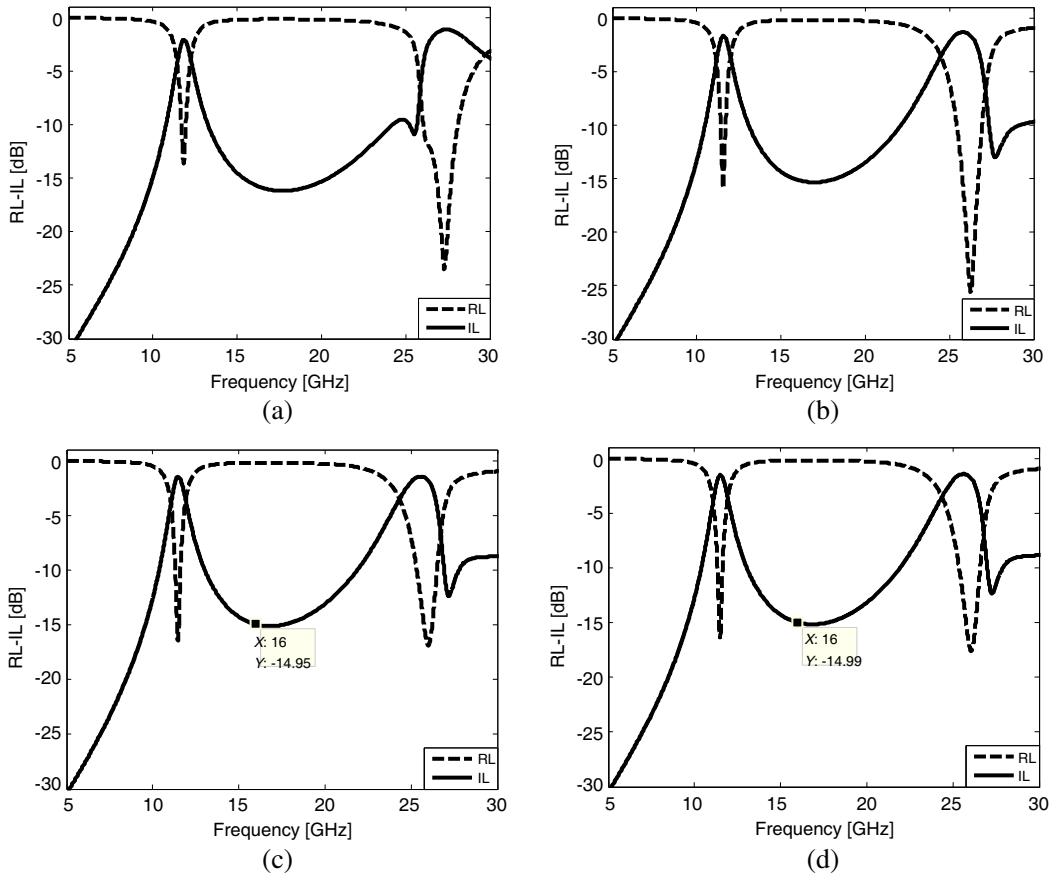

Figure 7. Insertion loss (full curve) and return loss (dashed curve) of (a) the resonator without fractal geometry, (b) the first iteration fractal resonator, (c) the second iteration fractal resonator and (d) the third iteration fractal resonator.

Table 3. First band simulated parameters for different iterations of fractal resonators.

Resonator parameters	***Zero Order***	***First Order***	***Second Order***	***Third Order***
f_1 (GHz)	11.84	11.59	11.57	11.47
Bandwidth, BW (GHz)	1.07	1.02	1	1
Insertion Loss, IL (dB)	2.11	1.63	1.58	1.48
Return Loss, RL (dB)	13.62	15.38	16.33	16.41

Table 4. Second band simulated parameters for the different iterations of fractal resonators.

Resonator Parameters	***Zero Order***	***First Order***	***Second Order***	***Third Order***
f_2 (GHz)	27.3	25.82	25.7	25.64
Bandwidth, BW (GHz)	-	2.68	2.54	3.03
Insertion Loss, IL (dB)	1.15	1.33	1.45	1.45
Return Loss RL (dB)	23.49	25.58	17.60	16.87

loss and minimum return loss. The simulated second iteration fractal resonator operates at 11.57 GHz and 25.7 GHz, with bandwidth of 1 GHz and 2.54 GHz, respectively. The first pass-band has a maximum insertion loss IL = 1.58 dB and a minimum return loss RL = 16.33 dB, while the second pass-band has a maximum insertion loss and a minimum return loss IL = 1.45 dB and RL = 17.60 dB, respectively. The

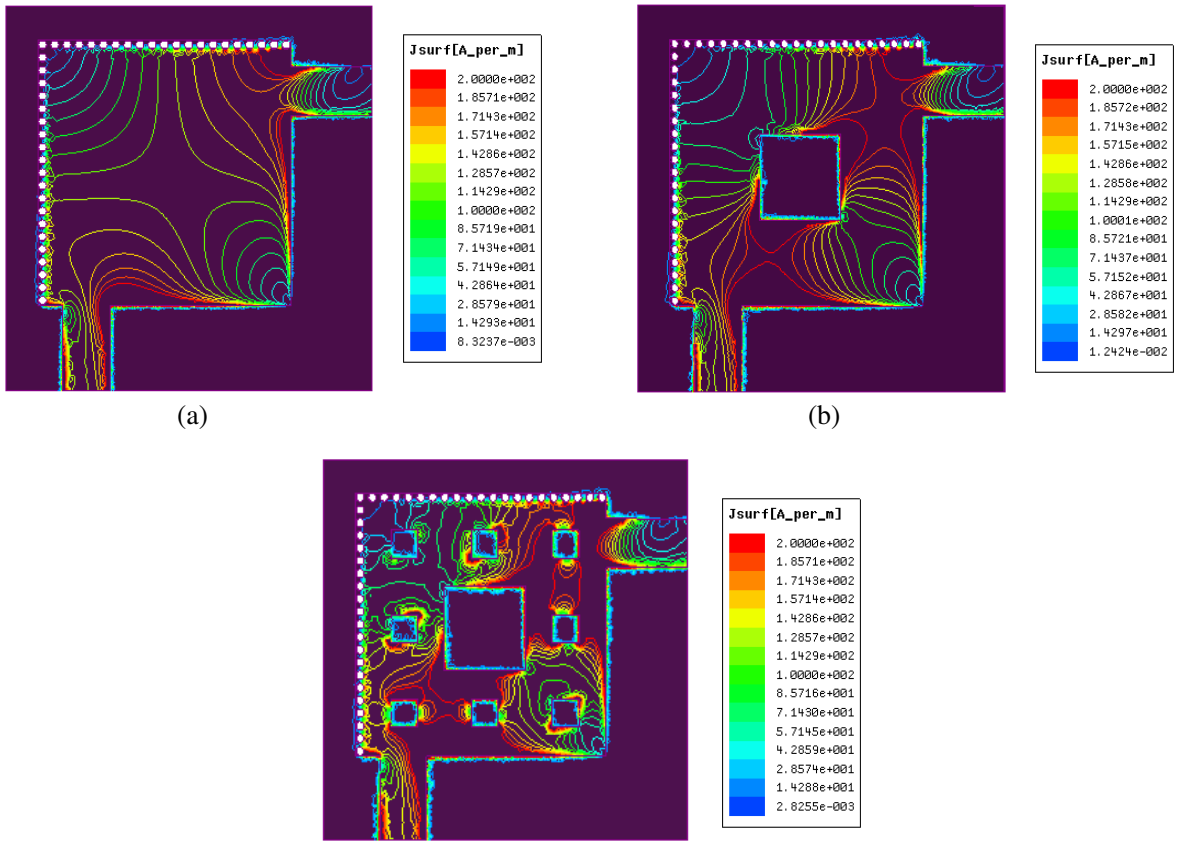

Figure 8. Current density contour plot of (a) the resonator without fractal geometry at frequency $f_1 = 11.84\,\text{GHz}$, (b) the first iteration fractal resonator at frequency $f_1 = 11.59\,\text{GHz}$, (c) the second iteration fractal resonator at frequency $f_1 = 11.57\,\text{GHz}$.

width of the stop-band between the first and second bands is close to 12 GHz. The simulated second iteration fractal resonator performance is very good and quite similar to those of third order one, the latter having a more sophisticated geometry than the former. Therefore, the resonator without fractal geometry, the first order and second order ones are chosen as prototypes to be constructed.

4. EXPERIMENTAL RESULTS

The zero, first and second iteration fractal resonators have been fabricated in SomacisS.p.A. via standard PCB fabrication technology [26–32], see Figures 9(a)–9(c). The total size of the resonator, including the input/output feed lines, is $3.2\,\text{cm} \times 3.2\,\text{cm}$. The zero-order resonator has been constructed for comparison; the third-order resonator has not been fabricated since by simulation, it exhibits characteristics quite similar to those of the second-order one. The resonators have been characterized by using a Agilent N5224A vector network analyzer. Figures 10(a)–10(b) illustrate both the measured and simulated IL and RL versus the frequency for the zero iteration fractal resonator.

The first band 10(a) is obtained close to 11.8 GHz, and the measured frequency response is in excellent agreement with simulation. The second band 10(b) of the resonator without fractal geometry, as expected, does not exhibit good characteristics; a slight frequency shift of the measured response with respect to the simulated one is apparent. Figures 10(c)–10(d) depict both the measured and simulated IL and RL versus the frequency of the first iteration fractal resonator. For the first band 10(c) the measured frequency response is, as in the previous case, in excellent agreement with simulation.

The second band 10(d) of the first iteration resonator has good characteristics, even if a frequency

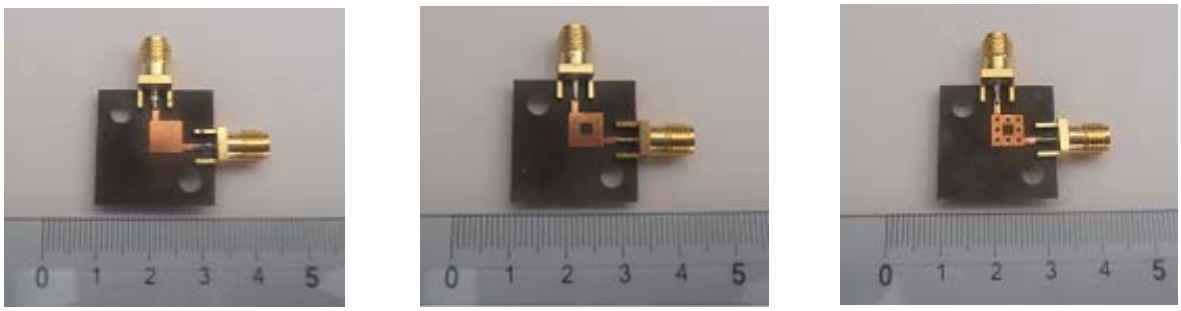

(a) (b) (c)

Figure 9. Prototype: (a) zero iteration fractal resonator, (b) first iteration fractal resonator, (c) second iteration fractal resonator.

shift of the measured response with respect to the simulated one is apparent as it has been observed for the zero iteration case.

Similar results are obtained for the second iteration fractal resonator as shown in Figures 10(e)–10(f). Therefore, both the first and second iteration resonators allow a good dual-band operation. The discrepancy, i.e., frequency shift, between the measured and simulated second band could be due to i) a displacement of dielectric constant frequency dispersion of the substrate in comparison with its nominal value used in simulation; more precisely, the simulation code HFSS allows to consider Rogers Duroid 5880 dielectric constant versus the frequency and the substrate thickness but both these values are nominal ones and in actual case slight differences can occur; ii) a critical behavior of the QSIWR resonator at high frequency, due to the open sides; in other words the QSIWR geometry has been considered to reduce four time in size the resonator area with respect to that of SIWR but the two sides 1, 2 (see Figure 2(b)) have been open, in actual cases this can lead to electromagnetic field leak and to a reactive behavior; iii) the behavior of the used connectors by increasing the frequency, since the soldered SMA connector geometry is slightly different from the simulated one and electromagnetic field radiation can occur at high frequency.

The characteristics of first and second iteration fractal resonators are listed in Table 5 and Table 6. The second iteration fractal resonator exhibits slight higher performance. It shows the first and second bands centered at $f_1 = 11.33\,\text{GHz}$ and at $f_2 = 23.67\,\text{GHz}$, the corresponding bandwidths being $\text{BW} = 1.15\,\text{GHz}$ and $\text{BW} = 2\,\text{GHz}$, respectively.

Table 5. Measured parameters of the first iteration fractal resonator.

Resonator parameters	***First Band***	***Second Band***
$f_{1,2}$ (GHz)	11.39	23.69
Bandwidth, BW (GHz)	1.22	2.18
Insertion Loss, IL (dB)	1.62	2.16
Return Loss, RL (dB)	20.16	17.96

Table 6. Measured parameters of the second itaration fractal resonator.

Resonator Parameters	***First Band***	***Second Band***
$f_{1,2}$ (GHz)	11.33	23.67
Bandwidth, BW (GHz)	1.15	2
Insertion Loss, IL (dB)	1.36	1.97
Return Loss, RL (dB)	24.46	< 30

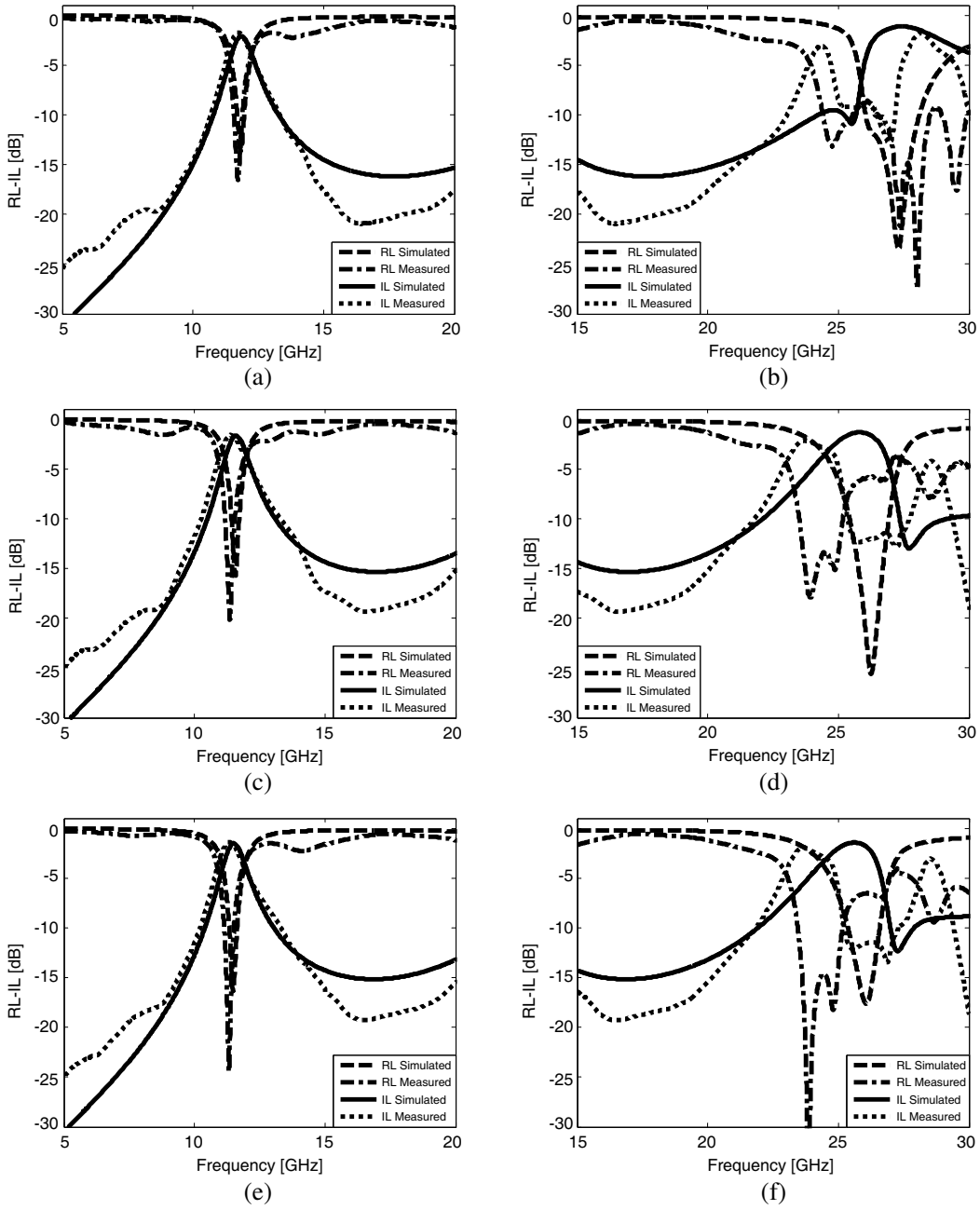

Figure 10. Comparison between measured and simulated IL, RL versus the frequency for: the zero iteration fractal resonator, (a) first band, (b) second band; first iteration fractal resonator: (c) first band, (d) second band; second iteration fractal resonator: (e) first band, (f) second band.

5. CONCLUSION

In this work, a SIW double-band square single resonator with Sierpinski carpet fractal geometry is proposed. High compactness is obtained with the adoption of a quarter SIW Resonator (QSIWR) geometry. The fractal technique is used to improve the performances of the resonator and introduce the dual-band operation.

An accurate electromagnetic investigation is made, for the different fractal iteration resonators, by using a full wave finite element method solver (Ansoft HFSS). The resonator characteristics have

been optimized by considering the bandwidth, minimum insertion loss, maximum return loss and stop band rejection. The zero, first order and second order fractal resonators have been constructed via a standard PCB fabrication technology, on a single layer of 0.381 mm thick Rogers Duroid 5880. The simulated and measured characteristics are in good agreement. A frequency shift between the simulated and measured second bands occurs. However, both the first and second order resonators allow a good dual band operation.

The best performance is obtained for the second iteration one. It exhibits the first and second bands centered at $f_1 = 11.33\,\text{GHz}$ and at $f_2 = 23.67\,\text{GHz}$, and the corresponding bandwidths are $\text{BW} = 1.15\,\text{GHz}$ and $\text{BW} = 2\,\text{GHz}$, respectively. These resonators can be employed to fabricate pass band filters for satellite communication and multiband filtering applications.

ACKNOWLEDGMENT

This work has been partially supported within the MIUR plans: PON01 01224 "Sviluppo di tecnologie in guida d'onda integrata (SIW) per applicazioni ICT a microonde"; PONa3 00298 "Potenziamento delle strutture e delle dotazioni scientifiche e tecnologiche del polo scientifico e tecnologico Magna Grecia"; PON02_00576_3329762 Sistemi avanzati mini-invasivi di diagnosi e radioterapia" AMIDERHA.

REFERENCES

1. Hao, Z. C., W. Hong, J. X. Chen, X. P. Chen, and K. Wu, "Planar diplexer for microwave integrated circuits," *IEEE Proc. Microw. Antennas Propag.*, Vol. 152, 455–459, 2005.
2. Hao, Z. C., W. Hong., J. X. Chen, H. X. Zhou, and K. Wu, "Single-layer substrate integrated waveguide directional couplers," *IEE Proc. Microw. Antennas Propag.*, Vol. 153, No. 5, 426–431, Oct. 2006.
3. Kazemi, R., A. E. Fathy, S. Yang, and R. A. Sadeghzadeh, "Development of an ultra wide band GCPW to SIW transition," *2012 IEEE Radio and Wireless Symposium (RWS)*, 171–174, 2012.
4. Cong, Z., P. Wang, and P. Li, "Analysis and experiment of transition between micro-strip and a miniaturization substrate integrated waveguide (SIW)," *7th International Symposium on Antennas, Propagation & EM Theory, ISAPE'06*, 1–4, Oct. 2006.
5. Bozzi, M., L. Perregrini, K. Wu, and P. Arcioni, "Current and future research trends in substrate integrated waveguide technology," *Radio Engineering*, Vol. 18, No. 2, 201–209, Jun. 2009.
6. Sabariah, S., B. H. Ahmad, and A. R. B. Othman, "A review of substrate integrated waveguide (SIW) bandpass filter based on different method and design," *IEEE APACE*, 210–215, Dec. 2012.
7. Tang, H. J., W. Hong, Z. C. Hao, J. X. Chen, and K. Wu, "Optimal design of compact millimetre-wave SIW circular cavity filters," *Electronics Letters*, Vol. 41, No. 19, 2005.
8. Chen, X. P. and K. Wu, "Substrate integrated waveguide cross-coupled filter with negative coupling structure," *IEEE Trans. on Microwave Theory and Techniques*, Vol. 56, No. 1, 142–149, 2008.
9. Zhang, Y. L., W. Hong, K. Wu, J. X. Chen, and Z. C. Hao, "Development of compact bandpass filters with SIW triangular cavities," *IEEE APMC*, 2005.
10. Xiao, J. K. and X. P. Zu, "Dual-band bandpass filter using right-angled triangular resonator," *IEEE Cross Strait Quad-Regional Radio Science and Wireless Technology Conference*, 690–695, 2011.
11. Szydlowiski, L., A. Lamecki, and M. Mrozowski, "Coupled-resonator waveguide filter in quadruplet topology with frequency-dependent coupling — A design based on coupling matrix," *IEEE Microwave and Wireless Components Letters*, Vol. 22, No. 11, 553–555, Nov. 2012.
12. Szydlowiski, L., A. Lamecki, and M. Mrozowski, "A novel coupling matrix synthesis technique for generalized Chebyshev filters with resonant source-load connection," *IEEE Transactions on Microwave Theory and Techniques*, Vol. 61, No. 10, 3568–3577, Oct. 2013.
13. Szydlowski, L., N. Leszczynska, A. Lamecki, and M. Mrozowski, "A substrate integrated waveguide (SIW) bandpass filter in a box configuration with frequency-dependent coupling," *IEEE Microwave and Wireless Component Letters*, Vol. 22, No. 11, 556–558, Nov. 2012.

14. Sun, S. J., T. Su, K. Deng, B. Wu, and C. H. Liang, "Compact microstrip dual-band bandpass filter using a novel stub-loaded quad-mode resonator," *IEEE Microwave and Wireless Components Letters*, Vol. 23, No. 9, 465–467, Sep. 2013.
15. Kufa, M. and Z. Raida, "Lowpass filter with reduced fractal defected ground structure," *Electronics Letters*, Vol. 49, No. 3, Jan. 2013.
16. Omar, M. and M. J. Mughal, "Behavior of electromagnetic waves at dielectric fractal-fractal interface in fractional spaces," *Progress In Electromagnetics Research M*, Vol. 28, 229–244, 2013.
17. Asad, H., M. Zubair, and M. J. Mughal, "Reflection and transmission at dielectric-fractal interface," *Progress In Electromagnetics Research*, Vol. 125, 543–558, 2012.
18. Mandelbrot, B. B., *The Fractal Geometry of Nature*, W. H. Freeman and Company, New York, 1977.
19. Xiao, J.-K., X.-P. Zu, X. Li, and L. Tian, "Right-angled triangular patch resonator and filter with fractal hole," *Progress In Electromagnetics Research B*, Vol. 40, 141–158, 2012.
20. Liu, B., Y. S. Mezaal, H. T. Eyyuboglu, and K. A. Jawad, "New dual band dual-mode microstrip patch bandpass filter designs based on Sierpinski fractal geometry," *3rd International Conference on Advanced Computing and Communication Technologies (ACCT-2013)*, 2013.
21. Liu, B., W. Hong, Y. Zhang, H. J. Tang, X. Yin, and K. Wu, "Half mode substrate integrated waveguide 180° 3-dB directional couplers," *IEEE Transactions on Microwaves Theory and Tecniques*, Vol. 55, No. 12, 2586–2592, Dec. 2007.
22. Zhang, Z., N. Yang, and K. Wu, "5-GHz bandpass filter demonstration using quarter-mode substrate integrated waveguide cavity for wireless systems," *IEEE*, 95–97, 2009.
23. Yang, G., W. Liu, and F. Liu, "A compact C-band bandpass filter using one eighth substrate integrated waveguide resonator," *IEEE International Conference on Microwave and Millimeter Wave Technology (ICMMT)*, Vol. 2, 1–4, 2012.
24. Jin, C. and Z. Shen, "Compact triple-mode filter based on quarter-mode substrate integrated waveguide," *IEEE Transactions on Microwave Theory and Techniques*, Vol. 62, No. 1, 37–45, Jan. 2014.
25. Xu, F. and K. Wu, "Guided-wave and leakeage characteristics of substrate integrated waveguide," *IEEE Transactions on Microwave Theory and Tecniques*, Vol. 53, No. 1, 66–73, Jan. 2005.
26. Anguerra, J., J. P. Daniel, C. Borja, J. Mumbrù, C. Puente, T. Leduc, K. Sayegrih, and P. Van Roy, "Metallized foams for antenna design: Application to fractal-shaped Sierpinski-carpet monopole," *Progress In Electromagnetics Research*, Vol. 104, 239–251, 2010.
27. Castellano, T., O. Losito, L. Mescia, M. A. Chiapperino, G. Venanzoni, D. Mencarelli, G. Angeloni, C. Renghini, P. Carta, and F. Prudenzano, "Feasibility investigation of low cost substrate integrated waveguide (SIW) directional couplers," *Progress In Electromagnetics Research B*, Vol. 59, 31–44, 2014.
28. Losito, O., L. Mescia, M. A. Chiapperino, et al., "X-band SIW cavity-backed patch antenna for radar applications," *EuMW 2013*, Nuremberg, Germany, Oct. 6–11, 2013.
29. Calò, G., A. D'Orazio, M. De Sario, L. Mescia, V. Petruzzelli, and F. Prudenzano, "Tunability of photonic band gap notch filter," *IEEE Transactions on Nanotechnology*, 273–284, 2008.
30. D'Orazio, A., M. De Sario, V. Marocco, V. Petruzzelli, and F. Prudenzano, "Photonic crystal drop filter exploiting resonator cavity configuration," *IEEE Transactions on Nanotechnology*, 10–13, 2008.
31. Losito, O., L. Mescia, D. Mencarelli, G. Venanzoni, and F. Prudenzano, "SIW cavity-backed patch antenna for Ku band applications," *7th European Conference on Antennas and Propagation (EUCAP 2013)*, 3095–3098, 2013.
32. Castellano, T., O. Losito, L. Mescia, M. A. Chiapperino, G. Venanzoni, D. Mencarelli, G. Angeloni, C. Renghini, P. Carta, P. Potenza, and F. Prudenzano, "Substrate integrated waveguide fixed phase shifter for 90±-degree directional coupler," *2013 IEEE Proceeding International Conference on Microwaves, Communications, Antennas and Electronic Systems (COMCAS 2013)*, 2013.